

Fatigue of Epoxy α -Zirconium Phosphate Nanocomposites

B.R. Varadharajan, W.N.P. Hung and H-J. Sue

Department of Mechanical Engineering
Texas A&M University, College Station, TX 77843

Abstract

This study aims at understanding the fatigue behavior and fracture mechanisms of Epoxy/ α -ZrP nanocomposites. Due to size constraints, a new fatigue testing technique was implemented. The fatigue stress and fatigue life of different nanocomposite specimens were plotted in a traditional stress-life (S-N) curve. Experimental results show that fatigue life of filled epoxy nanocomposite is more than that of the unfilled epoxy composite. This improvement in fatigue resistance can be attributed to the presence of reinforced core-shell rubber and ZrP nanoparticles which increase the fracture toughness and the tensile strength of the composite by hindering the propagation of crack.

Introduction

Polymer nanocomposites promise significantly better physical and mechanical properties than conventional micrometer-scale inorganic filler reinforced polymer nanocomposites. Though clay nanocomposites were characterized earlier and fundamental structure-property relationships were studied, the results obtained were ambiguous due to incomplete exfoliation of these nanocomposites. Epoxy/ α -ZrP nanocomposites possess better exfoliation properties and experimental parameters can be better controlled. Mechanical properties characterization of these nanocomposites will provide clear fundamental understanding of their behavior.

Nanocomposites with epoxy matrix and ZrP nanofillers are relatively new to the field of composite materials. Tensile testing of this material was carried out on clay nanocomposites¹. The modulus of clay nanocomposites was characterized and modeled as a function of different parameters that includes exfoliation ratio, matrix modulus and matrix Poisson ratio by subjecting the specimen to tensile loading. It was identified that with increase in exfoliation ratio, the Young's modulus increased for a constant value of clay concentration. It was inferred that stiffness enhancement was more for a matrix in a rubbery state (that is, high clay to matrix modulus ratio). Also a substantial increase in composite modulus occurs as the matrix's Poisson ratio increases. Fracture behavior of

clay nanocomposites in tension was studied and the morphological impact on the fracture mechanisms was explained². Stress concentration factor of the nanocomposites was plotted against clay concentration. The graph showed that at low clay concentration (<3.5 wt %) there was no significant improvement in fracture toughness (K_{IC}) as the clay particles remain isolated. As the clay concentration increases, the decrease in interparticle distance improves the fracture behavior. Tensile fracture behavior of Epoxy/a-ZrP nanocomposites with and without core shell rubber (CSR) was also studied. The CSR provides additional toughening characteristics to the composite. In the absence of the CSR, there is no distinguishable change in fracture toughness of the nanocomposite. However when CSR is utilized for toughening, significant increase in K_{IC} is observed. This is found out to be due to a mechanism named cavitation that the CSR undergoes. The cavitation of CSR particles near the wake of crack tip triggers massive shear banding of the matrix, thereby absorbing much of the energy that is being applied. This increases the fracture toughness of the material. Though research on tensile fracture behavior of Clay/epoxy and ZrP/epoxy nanocomposites has been carried out, no effort has been made to study the effect of cyclic load on epoxy/a-ZrP nanocomposites. The present study aims at understanding the fatigue fracture behavior and the ensuing crack propagation mechanism of these nanocomposites.

Experiments

A new fatigue testing technique was implemented due to size and material constraints. Cantilever shaped specimens were subjected to cyclic flexural loading of varying amplitudes from a vibration table that was excited with a sinusoidal wave from a function generator. The standard fatigue testing machines like single-ended rotating cantilever machine subjected the specimen to rotational bending resulting in alternate tension and compression of the outer fibers. This can be compared with our experimental setup in which the specimen experiences flexural bending and undergoes similar tension and compression alternatively.

A typical test specimen was machined from pre-molded composite plates. A Buehler ISOMET low speed diamond saw was used to precisely cut the plates with minimum alteration of the sample microstructure. The dimension of each specimen was 13 x 3 x 1.52 mm³. A 1.0 mm diameter hole was carefully drilled at the center of the beam using a Bridgeport Model 8F milling machine that equipped with a digital position reader at 1 μ m resolution. The hole was located away from the clamped end and at a distance of 8.5mm from the free end of the beam. It acted as the stress raiser with a known stress concentration factor to accelerate the fatigue test and eliminate inconsistent clamping effect at the end of the cantilever specimen. The testing frequency was capped at 10 Hz so that thermal degradation will not be a factor in the fatigue test. Figure 1 below shows a schematic of the experimental setup. A cantilever specimen was subjected to flexural bending with the help of a minishaker. Operational frequency of 10 Hz was provided by a frequency generator to the minishaker and the amplitude of vibration was verified with an oscilloscope as peak-peak voltage. Gain control of the power amplifier was kept constant

throughout the experiments. The voltages corresponding to maximum and minimum amplitudes and those in between were determined for that gain control. The cursor option in the oscilloscope helped in identifying the peak-peak voltage value for the corresponding amplitude.

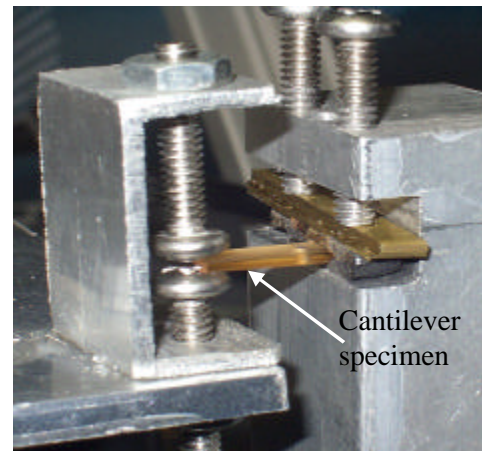
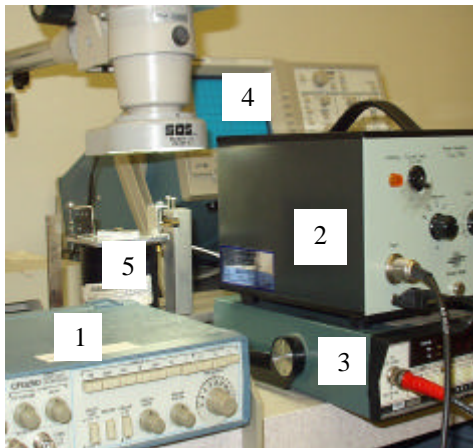
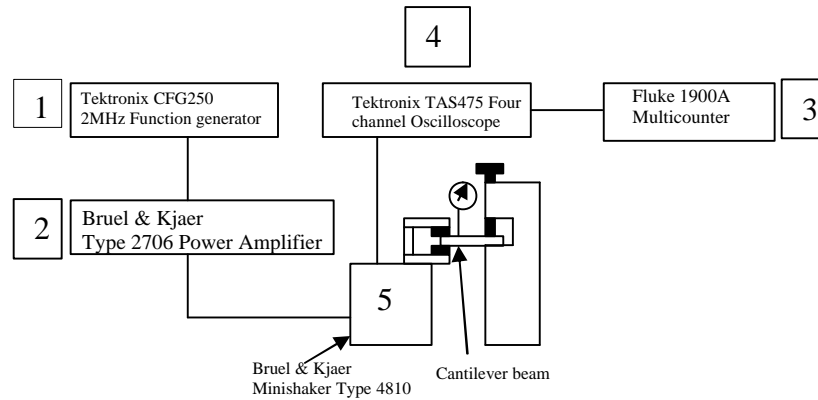


Figure 1: Schematic and photograph of experimental setup.

The system was calibrated before the experimental set-up was performed. Gain control was kept constant and an operating frequency of 10 Hz was maintained throughout. The graph below (Figure 2) shows the peak-peak voltage obtained from the oscilloscope against the table displacement measured using a dial gauge with a resolution of $12.5 \mu\text{m}$ (0.0005 in) without mounting the specimen. This graph helps us in obtaining table displacement for any voltage. The dial gauge was also used in measuring tip displacement for bending stress calculation. The results obtained are discussed in next section.

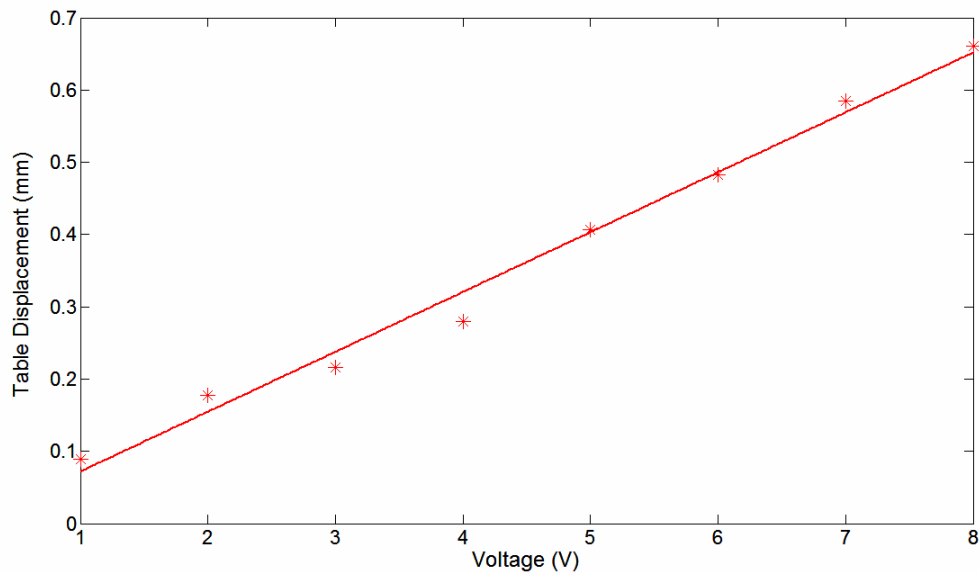


Figure 2: System calibration.

Results and Discussions

The stress acting at any point in the beam is calculated in three ways. Static bending stress is calculated using strength of material approach while Rayleigh-Ritz method is used to determine dynamic stress on the beam. Both methods are discussed in the appendix of this paper. Finally, finite element stress analysis is carried out using ABAQUS for comparison with the above calculated results.

Figure 3 shows the finite element stress analysis for a maximum tip displacement of 0.685 mm. It can be seen that the maximum von Mises stress at the hole edges is 47.75 MPa. The maximum bending (normal) stress calculated by beam theory for the same displacement is 48.04 MPa. The minor error is due the estimated theoretical value of the stress concentration factor at the hole. Referring to Table 1, it can be seen that the static and simulated stress values match closely while the calculated dynamic stress is about 20% higher than the static stress. It was found out during the calculations that the system does not act dynamically. Instead it experiences pseudo-static loading. This can be inferred by comparing the calculated natural frequencies with the operating frequency of the system. It is obvious that the system does not get excited to its modes of vibrations. Also the mass matrix, which gives the inertia term that plays an important role in dynamics, is very small compared to the stiffness matrix leading us to the conclusion that there is negligible dynamic force involved and hence the static stress calculated using concepts of strength of material approach should give an accurate data. Thus the difference in stress values is due to the inaccuracy of Ritz method with regard to this system.

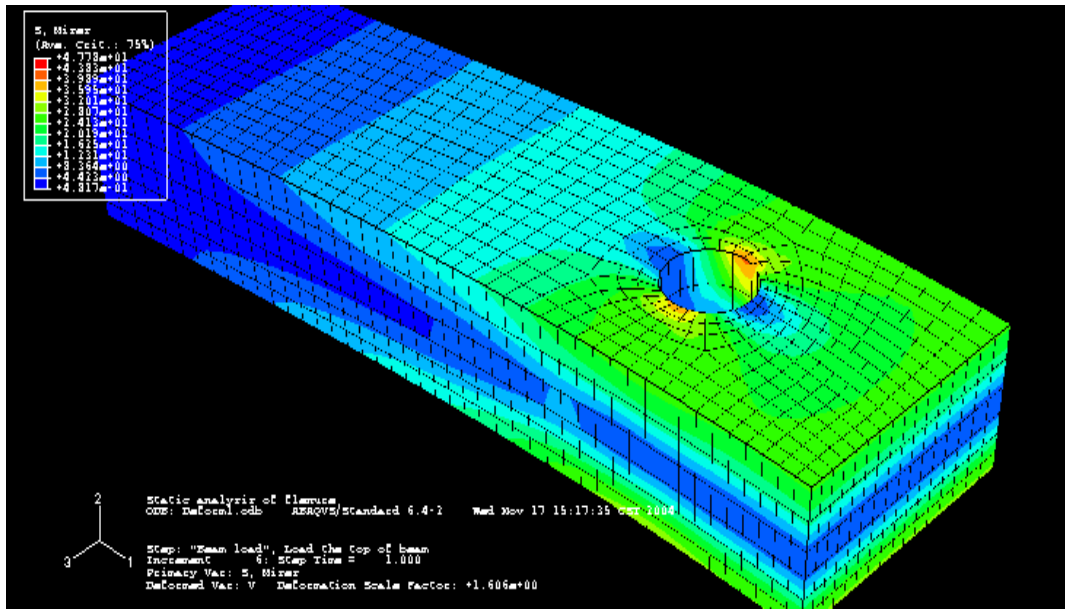


Figure 3: Simulation of bending stress for Neat Epoxy for a maximum cantilever tip displacement of 0.685 mm.

Table 1: Calculated bending, dynamic and simulated stresses.

Material	Peak-peak amplitude (V)	Tip displacement (mm)	Bending stress (MPa)	Ritz dynamic stress (MPa)	Simulated stress (MPa)
Neat Epoxy	1.10	0.152	10.66	13.73	TBD
	2.20	0.279	19.57	25.18	19.45
	6.64	0.398	27.87	35.87	27.76
	9.00	0.462	31.73	41.64	32.23
	11.00	0.533	37.36	48.07	37.2
	12.00	0.591	41.40	53.27	43.22
	13.42	0.685	48.04	61.74	47.75
M-ZrP/Epoxy	7.00	0.444	41.46		
	8.00	0.495	46.01		
	10.00	0.940	87.53		
CSR/M-ZrP/Epoxy	10.00	0.533	47.18		

The effect of different particle sizes of silicon on the fatigue strength of PMMA/silicon particulate composite was analyzed in another research⁴. It was inferred that an increasing of reinforcement volume fraction would increase the fatigue life of the composite. Experimental data shows fatigue life of reinforced nanocomposite (with 2.0% vol of a-ZrP and 20 mmol of Jeffamine) samples is approximately one order of magnitude longer than that of neat epoxy samples. From a study that was conducted

earlier on Epoxy/ZrP nanocomposites, it was inferred that addition of ZrP fillers increases the tensile modulus by 50% and the tensile strength by 10%. The trend is similar to fatigue results of common polymers and metals, i.e. the material fatigue strength is proportional to the material tensile strength. Figure 4 plots the experimental fatigue data of the epoxy and the epoxy reinforced with ZrP nanoparticles. Like other polymers, these polymer-based nanocomposites do not exhibit a fatigue endurance limit as commonly observed for metals and their alloys.

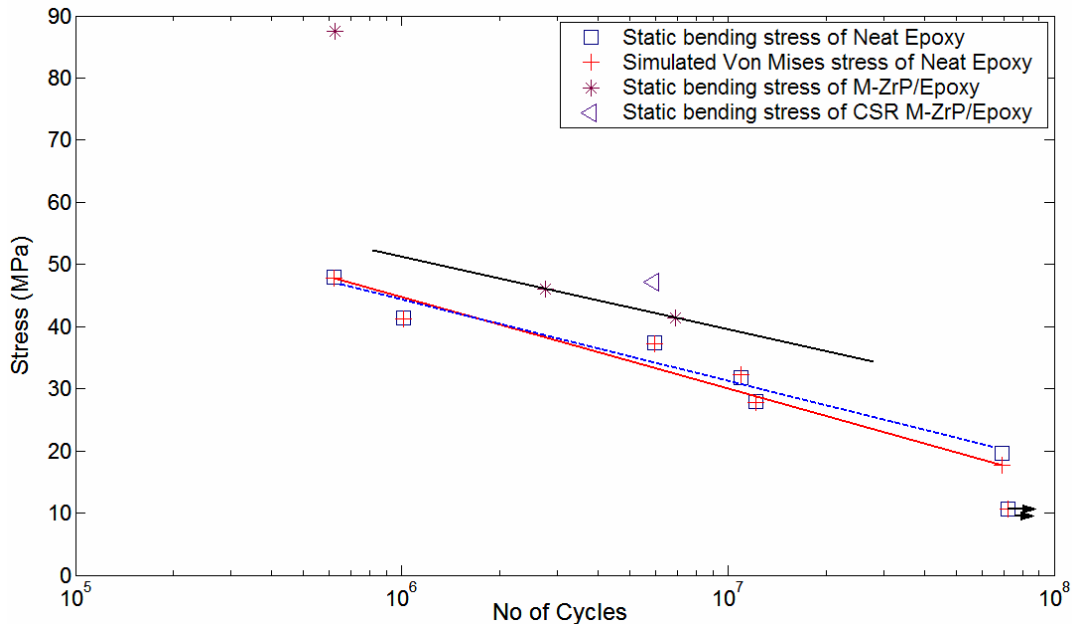
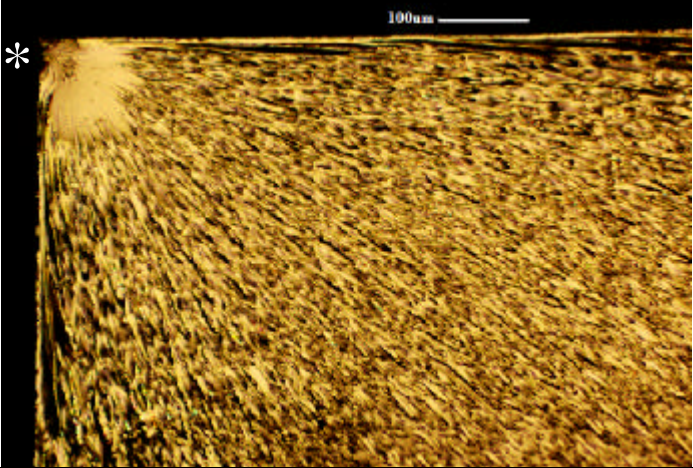
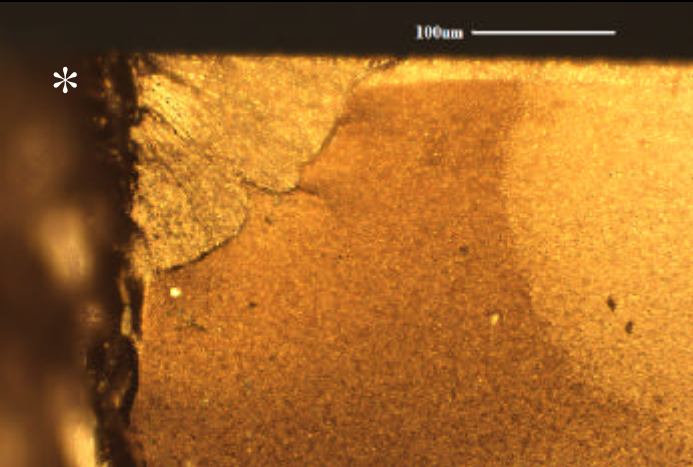
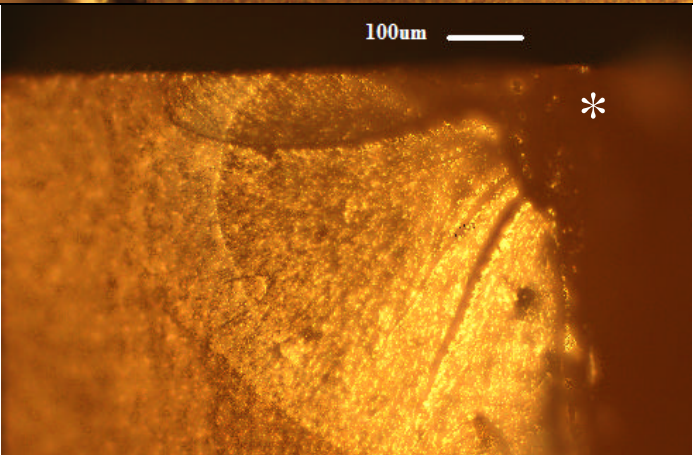


Figure 4: The S-N plot for Neat epoxy and Epoxy/ZrP nanocomposites.

Figure 4 shows that fatigue life of filled epoxies is enhanced as compared to the unfilled epoxy. This improvement in the behavior of reinforced nanocomposite can be attributed to the presence of ZrP nanoparticles and CSR particles which increase the fracture toughness of the material by hindering the propagation of crack. Higher fatigue strength of CSR modified nanocomposite can be attributed to the cavitation process by which the rubber particles near the wake of crack tip elongate thereby absorbing much of the energy resulting in increased fracture toughness. The improvement in fatigue life of reinforced nanocomposite can also due to the presence of ZrP nanoparticles. Although TEM examination showed some delamination of matrix and particle in the plastic zone in front of a crack tip, the nanoparticles effectively retard the crack initiation and improve the overall fatigue life. Figure 5 below shows the fractured surfaces of Neat Epoxy, and epoxy filled with CSR and ZrP nanoparticles.

	<p>Figure 5a: Fracture surface of epoxy. Fatigue failure after 122 millions cycles at 27 MPa bending stress. The "*" indicates the crack origin at the drilled hole.</p>
	<p>Figure 5b: Fracture surface of M-ZrP /Epoxy. Fatigue failure after 6.2 millions cycles at 87 MPa bending stress. The "*" indicates the crack origin at the drilled hole.</p>
	<p>Figure 5c: Fracture surface of CSR/M-ZrP/Epoxy. Fatigue failure after 59.4 millions cycles at 59 MPa bending stress. The "*" indicates the crack origin at the drilled hole.</p>

A typical fractograph of neat epoxy shows the point of crack initiation followed by striations and beach marks that map instantaneous positions of crack tip during fatigue crack propagation. It will be verified with scanning electron microscopic and transmission electron microscopic examination the roles of reinforcing CSR and ZrP on the fatigue crack initiation and propagation. River like patterns follow the striations

which clearly indicate the path and direction of crack growth. Such fracture surfaces are similar to those that were observed in studies conducted earlier⁵. The fractographic surface of filled nanocomposite shows the point of crack initiation as well. However, there is a marked difference from that of neat epoxy in the region next to the crack initiation. Evidence of discontinuous crack growth can be seen from the stop-and-go crack fronts. This may be attributed to the presence of ZrP nanoparticles along the path of crack propagation which increases the fracture toughness of the material around that region reducing the speed of crack resulting in its stagnation and consequently in higher fatigue life as observed from the experimental results.

Summary and Conclusions

1. A new fatigue testing method was adopted to assess the fatigue life of small samples by oscillation the samples on a vibration system.
2. At testing frequency of 10 Hz, there was no evidence of thermal softening of any tested sample.
3. The fatigue life for neat epoxy is approximately one order of magnitude less than that of the M-a-ZrP/Epoxy.
4. There is no endurance limit for both materials as typical for most polymers and aluminum alloys.
5. It was postulated that the presence of ZrP nanofillers retards the crack initiation process, and probably hinders the crack advancement and consequently increases the fatigue life of the material. The CSR and its cavitation action absorb energy in front of a crack and effectively reduce the crack growth rate.
6. Fractographs of reinforced epoxy samples indicating discontinuous stop-and-go crack fronts also supports this reasoning. Fractographs of neat epoxy shows smooth facets which are typical of brittle materials.

Future Works

Experiments will be continued for specimens of different volume fraction of nanoparticles. The data points obtained will be used in plotting a complete S-N graph for comparison and design aid. Scanning and transmission electron microscopic examination of fractured surfaces will help to understand the role of the reinforcement in the fatigue crack initiation and propagation.

References

1. Luo J.J., Daniel I.M., 2003, Characterization and modeling of mechanical behavior of polymer/clay nanocomposites, *Comp Sci and Tech*, Vol. 21, pp. 1607-1616
2. Zerda A.S., Lesser A.J., 2001 Intercalated Clay nanocomposites: Morphology, mechanics and fracture behavior, *Journal of Pol Sci Part B*, Vol. 39, No.11 pp. 1137-1146.
3. Sue H.J., Gam K.T., Bestaoui N., Clearfield A., Miyamoto M., Miyatake N., 2004, Fracture behavior of a-zirconium phosphate-based epoxy nanocomposites, *Acta Materialia*, Vol.52, No.8, pp. 2239-2250.
4. Sue H.J., Gam K.T., Bestoui N., Spurr N., Clearfield A., 2004, Epoxy Nanocomposites Based on the Synthetic a-Zirconium Phosphate Layer Structure, *Chem. Mater*, Vol.16, pp 242-249.
5. Antunes F.V., Ferreira J.M., Costa J.D., Capela C., 2002, Fatigue life predictions in polymer particle composites, *International Journal of Fatigue*, Vol. 24, pp. 1095-1105..
6. Young R.J., 1980, Developments in Reinforced Polymers, edited by G. Pritchard, Applied Science, London.
7. Ginsburg J.H. 2001, Mechanical and Structural Vibrations -- Theory and applications, John Wiley and Sons.

BALAJI R. VARADHARAJAN

Balaji is a graduate student at the Department of Mechanical Engineering at Texas A & M University. His research interests include stress/strain analysis and finite element methods.

WAYNE N.P. HUNG

Dr. Hung currently serves as an Associate Professor of the Department of Engineering Technology & Industrial Distribution, and the Department of Mechanical Engineering at Texas A&M University. He is a member of ASPE, and SME. His research interests include advanced materials and micro/nano manufacturing.

HUNG-JUE SUE

Dr. Sue a Professor at Department of Mechanical Engineering at Texas A&M University. Dr. Sue's research interests include nanocomposites and advanced polymers.

Appendix

Two approaches are presented here to calculate the stresses acting at the end of cantilever beam and near the hole location. The first method uses the classical beam theory while the second method is the Rayleigh-Ritz method that is used to calculate the dynamic stresses acting in the beam.

Static analysis

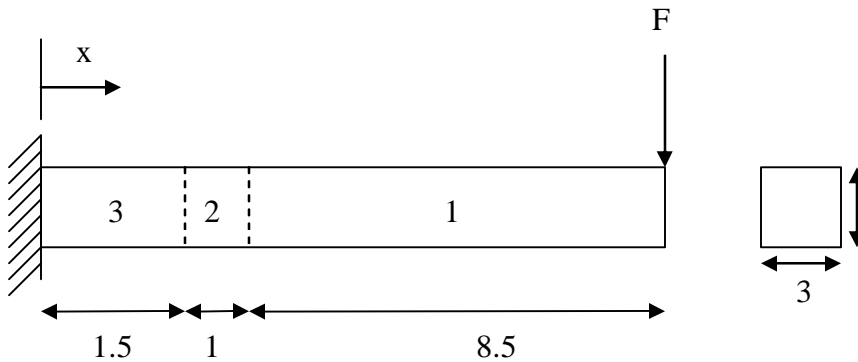
The following symbols are used in explaining this method

x = Location along the length of beam where the stress has to be calculated

l = Total length of the beam

P = Force acting at the tip of the beam

Considering the cantilever beam below



From the concepts of strength of materials,

$$\begin{aligned} \frac{dy}{dx} &= \int_0^{1.5} \frac{P(l-x)}{E \times 0.877} dx + \int_{1.5}^{2.5} \frac{P(l-x)}{E \times 0.585} dx + \int_{2.5}^{11} \frac{P(l-x)}{E \times 0.877} dx \\ &= \frac{P}{E \times 0.877} [1.5l - 1.125] + \frac{P}{E \times 0.585} [l - 2] + \frac{P}{E \times 0.877} [8.5l - 57.3] \end{aligned}$$

Substituting E for epoxy = 2.9GPa in the above equation, we get

$$\begin{aligned} \frac{dy}{dx} &= 0.0253P \\ \Rightarrow y &= 0.0253Px \end{aligned}$$

To get the maximum displacement which occurs at the tip of the beam, let $x = l$ and we get

$$y = 0.2783P$$

We now equate this equation for y with the tip displacement that was measured by the dial gage. For example, considering the second displacement state of the experiment,

$$0.2783P = 0.398$$

$$\Rightarrow P = 1.43N$$

We use this value of force to calculate the nominal stress and the stress acting near the hole.

$$s_{nom} = \frac{1.43 \times 8.5 \times 0.75 \times 12}{2 \times 1.52^3} = 15.57 MPa$$

$$\Rightarrow s_{hole} = 1.79 \times 15.57 = 27.87 MPa$$

Dynamic analysis

The following symbols are used in explaining this method

M = Mass matrix

K = Stiffness matrix

\dot{Q} = Force matrix

u = Displacement of the beam as a function of time and space

w_n = Natural frequencies of the beam

y_j = Basis function

Assuming no damping effect on the material,

$$[M] \left\{ \ddot{q} \right\} + [K] \left\{ q \right\} = \left\{ Q^* \right\}$$

For flexural displacement of bars, the expressions for M, K and Q are given as⁶

$$M_{nj} = M_{jn} = \int_0^L y_j y_n r A dx$$

$$K_{nj} = K_{jn} = \int_0^L EI \frac{dy_j}{dx} \frac{dy_n}{dx} \text{ and}$$

$$Q_j = \sum F y(x_F)$$

We choose the basis function as⁶

$$y_j = \left(\frac{x}{L} \right)^{j+1}$$

The Ritz series representation of displacement is given by

$$\begin{aligned} u(x,t) &= \sum_{j=1}^N y_j(x) q_j(t) \\ &= \sum_{j=1}^2 \left(\frac{x}{L} \right)^{j+1} \text{Re} \{ X_j e^{i\omega t} \} \end{aligned} \quad (1)$$

We need to calculate X at each of the natural frequencies of the system.

Considering the beam with a hole, the system can be divided into three parts. To derive an equation for this system, we have to use the multipart Ritz function. Using that method, we get

For $j, n = 1, 2$

$$M = \begin{bmatrix} 0.012 & 0.01 \\ 0.01 & 8.59 \times 10^{-3} \end{bmatrix}$$

and

$$K = \begin{bmatrix} 7.41 & 11.33 \\ 11.33 & 22.85 \end{bmatrix}$$

Considering the eigenvalue equation,

$[K] - \omega^2[M] = 0$ and substituting the M and K matrices from above, we get the natural frequencies as

$$\omega_1^2 = 0.0372 \times 10^4 \text{ rad/s}; \omega_2^2 = 3.5749 \times 10^4 \text{ rad/s}$$

For $\omega_1^2 = 0.0372 \times 10^4 \text{ rad/s}$,

$$\{X\} = \begin{bmatrix} 0.6499 & -0.3124 \\ -0.3124 & 0.1949 \end{bmatrix} \begin{Bmatrix} a \\ a \end{Bmatrix} = \begin{bmatrix} 0.3375a \\ -0.1175a \end{bmatrix} \text{ and}$$

For $\omega_2^2 = 3.5749 \times 10^4 \text{ rad/s}$,

$$\{X\} = \begin{bmatrix} 0.0529 & -0.0926 \\ -0.0926 & 0.1236 \end{bmatrix} \begin{Bmatrix} a \\ a \end{Bmatrix} = \begin{bmatrix} -0.0397a \\ 0.031a \end{bmatrix}$$

From (1)

$$u(x, t) = \text{Re}[U(x) \exp(i\omega t)], U(x) = \sum_{j=1}^2 \left(\frac{x}{L}\right)^{j+1} X_j$$

$$\Rightarrow U(x) = \left[\left(\frac{x}{L}\right)^2 \quad \left(\frac{x}{L}\right)^3 \right] \begin{bmatrix} 0.3375a & -0.0397a \\ -0.1125a & 0.031a \end{bmatrix}$$

$$\Rightarrow U(L) = 0.2163a$$

For the first case, tip displacement, $U = 0.0157 \text{ in} = 0.398 \text{ mm}$

$$\Rightarrow 0.2163a = 0.398$$

$$\Rightarrow a = 1.84N$$

This dynamic force is used in calculating the stress acting in the beam.

$$s_{nom} = \frac{1.84 \times 8.5 \times 0.75 \times 12}{2 \times 1.52^3} = 20.04 \text{ MPa}$$

$$s_{hole} = 1.79 \times 20.04 = 35.87 \text{ MPa}$$